An S-Shaped Aβ42 Cross-β Hexamer Embedded into a Lipid Bilayer Reveals Membrane Disruption and Permeability

Phuong H Nguyen, Philippe Derreumaux

A S-shaped Aβ42 Cross-β Hexamer Embedded into a Lipid Bilayer Reveals Membrane Disruption and Permeability

Phuong H Nguyen,[1] and Philippe Derreumaux [1,2*]

1 CNRS, Université Paris Cité, UPR 9080, Laboratoire de Biochimie Théorique, Institut de Biologie Physico-Chimique, Fondation Edmond de Rothschild, 13 rue Pierre et Marie Curie, 75005 Paris, France.

2 Institut Universitaire de France (IUF), 75005, Paris

ABSTRACT

The interactions of amyloid oligomers with membranes are known to contribute to cellular toxicity. Numerous *in vitro* experimental studies reported on the insertion of oligomers of different sizes that can induce cell membrane disruption, extract lipids and form ion-permeable transmembrane pores. The current repertoire of amyloid-beta (Aβ) membrane-inserted folds that was subject to high-resolution structure NMR spectroscopy and computer simulations is devoid of any cross-β fibrillar structure. In this study, we explored the dynamics of a S-shaped Aβ42 cross-β hexamer model inserted into a lipid bilayer membrane by two atomistic molecular dynamics simulations. The initial model is characterized by the hydrophobic residues at the central hydrophobic core (residues 17-21, CHC) and the C-terminus (residues 30-42) embedded into the membrane. We observed major structural secondary, tertiary and quaternary rearrangements leading to two distinct species, hexamer and two trimers, accompanied by membrane disruption and water permeation. The simulations show that some configurations, but not the majority, have the CHC and C-terminus hydrophobic residues exposed to solvent. Overall, our computational results offer new perspectives to understand the relationship between Aβ42 assemblies and membrane permeability.

1.INTRODUCTION

Neurogenerative diseases are associated with the misfolding and aggregation of intrinsically disordered proteins which lack stable secondary structures in the bulk solution and at the surface of membranes.[1-4] Numerous experimental studies explored the interactions of amyloid oligomers with membrane mimetic systems including liposomes, vesicles, micelles, monolayer and bilayer models and nanodiscs. They led to three membrane-induced toxicity models; the membrane destabilization model, the detergent (lipid extraction) model and the pore model,[5-12] which were demonstrated for amyloid-beta (Aβ) and tau oligomers[5,11,12] contributing to Alzheimer's disease, and α-synuclein oligomers linked to Parkinson's disease.[12]

The "channel hypothesis" of Alzheimer's disease dates back from the electrophysiological measurements performed in 1993 by Arispe et al.[13] Initially, they proposed the β-hairpin followed by a helix-turn-helix model of Aβ42 peptide to design three pore models, with the pore being formed either by the hairpins, middle helices or C-terminal helices.[14] Recently, they designed β-barrels of six hexamers and pores formed by several hexamers spanning the bilayer.[15]

On the basis of SDS-PAGE, circular dichroism and electrical recording, specific Aβ42 pore forming β-barrel tetramers with an inner diameter of 0.7 nm in dodecylphosphocholine (DPC) micelle conditions were reported.[16] A tetrameric β-barrel, consisting of two distinct β-hairpin motifs and an asymmetric arrangement of eight antiparallel β-strands with an inner of diameter of 0.7 nm, was found by atomistic replica exchange dynamics simulations (REMD) to be destabilized for Aβ40 compared to its Aβ42 counterpart in a membrane model, explaining the absence of ionic currents of Aβ40 in planar lipid bilayers.[17] Additional REMD simulations showed that the lower AD propensity of aged rodents, characterized by mutations R5G, Y10F and H13R compared to human sequence, might be correlated to its tetrameric β-barrel stability in a model membrane.[18] Another REMD simulation in a dipalmitoylphosphatidylcholine (DPPC) membrane showed that the wild-type Aβ42 sequence and its protective-disease A2T variant have similar propensity to form β-barrels.[19]

Other experimental studies showed that Aβ β-hairpin mimics form a triangular trimer unit that self-assembles into hexamers and dodecamers with annular pores, which are toxic toward

neuronally derived cells.[20] Ion mobility-mass spectrometry revealed formation of hexameric β-barrels in a membrane-mimicking environment.[21] Mass spectrometry and nuclear magnetic resonance (NMR) spectroscopy in DPC micelles at pH 9.0 provided the first high-resolution structure of Aβ42 tetramer and octamer and revealed edge conductivity pores as a mechanism for membrane damage. The tetrameric topology comprises a six stranded β-sheet core with the two external Aβ peptides forming β-hairpins.[22] Overall, a wide range of concentric β-barrels is consistent with image averaged electron micrographs.[23]

Inspired by many biological ion channels using α-helix bundles, simulations showed that trimer and tetramer of Aβ17-42 transmembrane α-helices are possible candidates to conduct Na^+ ions.[24] Apart from the organization in α-helix bundles and β-barrels made of β-hairpins to build pores, Nussinov et al. proposed, on the basis of atomic force microscopy (AFM) imaging and modelling, that Aβ17-42 pentamer with U-shaped fibrillar state is able to insert into the lipid bilayer.[25] The same strand-loop-strand fibril state was used to construct annular Aβ oligomers with a number of peptides varying between 12 to 36 and pore inner diameters varying between 2 and 4 nm. Molecular dynamics (MD) simulations in different lipid bilayers showed that pores made of 18 and 24 peptides with the C-terminal β-strands in contact with the lipid hydrophobic tails retained their morphologies.[26] Of note, there is a structural convergence among diverse, toxic β-sheet ion channels,[27] and the U-shaped conformation was also predicted by a basin-hoping global optimization and an oligomer generation procedure for 6- and 8-mers of Aβ42 peptide in an implicit membrane environment.[28] Overall, the repertoire of Aβ folds in membranes is diverse, and this is supported by REMD simulations which showed that Aβ11-40 trimer resulting from assembly of U-shaped fibril states or β-hairpins represents minimal seeds for the formation of amyloid fibrils, multiple β-rich aggregates and β-barrel pores in a membrane.[29]

Membrane disruption and lipid extraction by amyloid oligomers were assessed by many experiments. They were demonstrated by cryo-electron tomography from the interactions of the amyloid fibril ends of β2-microglobulin and membrane surface.[30] Nanoscale imaging experiments showed how Aβ42 fibrils displace the upper leaflet of the membrane as fibers laterally embed into the bilayer.[31] Membrane disruption by incorporated-Aβ40 oligomers in 1-palmitoyl-2-oleoyl-sn-glycero-3-phosphocholine (POPC) bilayers,[32] and incorporated-Aβ42 β-sheet tetramer

and octamer in DPC micelles and lipid bilayer[22] was also reported using solid-state and solution NMR spectroscopies, respectively.

Melacini et al. evidenced Aβ40 fibrils inserted into small unilamellar vesicles and lipid bilayers.[33] Combining wide-angle X-ray diffraction, solution NMR, dynamic light scattering, electron microscopy, ANS fluorescence and cell viability assays, they studied the toxic surfaces of Aβ40 that enable key interactions with the membrane. They found that toxicity scales with hydrophobic exposure of Aβ40 assemblies to solvent and their ability to interact with Aβ monomers and cell membranes. The central hydrophobic core (CHC, residues L17-A21) and the loop region (residues E22-K28) were found more accessible to monomer recognition in toxic Aβ assemblies.[33]

Many computational studies on the interactions of amyloid oligomers with membranes were reviewed in Ref.7. Recent MD simulations explored the interactions of Aβ dimers at the surface or inserted into a membrane. Strodel et al. showed that Aβ42 dimer-membrane interactions do not change the lipid order parameters of the neuronal membrane.[34] Miller et al. showed that inserted random/α-helix and U-shaped Aβ dimers disrupt a 1,2-dioleoyl-sn-glycero-3-phosphocholine (DOPC) membrane by locally decreasing the bilayer thickness.[35] Li et al. investigated the effect of Aβ42 dodecamer and fibril on the surface of a neuronal membrane. They showed that a dodecamer distorts the lipid membrane to a greater extent than fibril, and fibril does not change the membrane elastic properties.[36] Strodel et al. also found membrane permeation induced by U-shaped fibrillar trimers and tetramers of human islet amyloid polypeptide in bilayers of anonic dipalmitoylphosphatidylglycerol (DPPG) lipids.[37] Using Aβ42 tetramers with a U-shaped topology spanning residues 17-42 inserted into the membrane and all N-terminal residues 1-16 located in the bulk solution at the top leaflet of the membrane, Strodel et al. reported on the translocation of a few water molecules through POPC, DPPC and palmitoyloleoylphosphatidylglycerol (POPG) bilayers using 500 ns MD simulations. Variation of bilayer thickness from 3.5 to 4.1 nm without any membrane destabilization was reported.[38]

The question we ask in this study is how a lipid bilayer is affected by placing a naked fibril cross section into the membrane and vice versa at an atomistic level. To this end, we explored the dynamics of a hexamer S-shaped Aβ42 fibrillar model inserted into a membrane (Figure 1)

using atomistic MD simulations. The S-shaped fold, more disease-relevant than the U-shaped fold, displays a 3D structure with residues Q15-A42 forming a double horseshoe-like cross–β-sheet structure, and residues D1-H14 partially ordered and residues A2-H6 in a β conformation.[39] We used this molecular structure rather than a prevalent Aβ40 fibril polymorph from Alzheimer's disease brain tissue[40] because Aβ42 is known to be more toxic than Aβ40. Furthermore, the S-shape fold is shared by the amyloid fibrils of the human islet amyloid polypeptide (hIAPP).[41,42]

2. RESULTS AND DISCUSSION

2.1. Impact of Membrane on Aβ42 Secondary Structure and Intermolecular Interactions. We first report on the secondary structure averaged over all residues and along the amino acid sequence in the ss-NMR amyloid fibril and in the simulations. The β-strand/sheet content amounts to 53% in amyloid fibrils grown from AD brain with five β-regions spanning β1: A2-H6, β2: Q15-V18, β3: S26-K28, β4: A30-I32 and β5: V39-A42.[39] Averaged over the full trajectories, the (β-strand, helix, coil and turn) contents stabilize to (27.0, 0.0, 47.0 and 26.0%) in run 1 and (24.0, 1.0, 49.0 and 26.0%) in run 2. The β-strand, helix, coil and turn contents along the sequence averaged over the six chains are shown in Figure 2 using four consecutive time-windows. We see that the secondary structure along the sequence has almost converged between 500-2000 ns in each run. The membrane environment fully destabilizes the β1 and β3 strands (Figures 2A1-2B1) with a very high preference for coil/turn (Figures 2A3, 2A4, 2B3 and 2B4), modifies the β2 strand propensity with a 38% (run 1) and 74% (run 2) content, preserves the propensity of β4 strand (64% in run 1 and 75% in run 2) and reduces the β5 strand to residues 39 and 40. Run 1 is free of helix (Figure 2A2), while run2 displays 10% helix at residues 24-27 (Figure 2B2).

To explore the dynamics of the oligomer, we calculated the intermolecular side chain probability contact map between the trimer 1 and the trimer 2 as a function of time intervals (Figure 3). The ss-NMR fibril structure shows intermolecular side-chain M35-Q15 (region 1), and L17-M35 (region 2) contacts.[39] The MD-ensemble of conformations between 0 and 100 ns of both runs (Figure 3A-3E) reveal the two ss-NMR regions, but adds a few contact outliers between residues 34-36 (region 3). In run 1, the three contact regions are conserved in the time-interval

500-1500 ns (Figures 3B-3C), but only region 3 with the intermolecular M35-M35 non-native ss-NMR contact is present in the time-interval 1900-2000 ns (Figure 3D). This indicates that in run 1, the system remains a hexamer and has lost the symmetry of the ss-NMR fibril. In run 2, only the region 2 is conserved from 500 to 1500 ns (Figures 3F-3G), and the last 1900-2000 ns is free of any contacts (Figure 3H), indicating that the system has evolved to two separated trimers. Overall, the results provide evidence of the significant change in the secondary and quaternary structures of Aβ oligomers embedded in a membrane model consisting of DOPC lipids.

The contribution of hexamer Aβ species to the development of AD pathology was reported by several studies. Bowers et al., using high resolution AFM to image oligomer populations, found that Aβ42 hexamers and dodecamers become the dominant oligomers after peptide solubilization, even at 1 μM concentrations and 5 min incubation times.[43] Aβ42 pentamers/ hexamers were found to be the smallest detectable oligomers in the bulk solution using sedimentation velocity centrifugation, small angle neutron scattering and molecular modelling.[44] Hexamers in the bulk solution are largely disordered and random/coil. The presence of hexamers was also detected in transgenic mice brains exhibiting human Aβ pathology and in the cerebrospinal fluid (CSF) of AD patients. Furthermore, cell-derived hexameric Aβ seeded other human Aβ forms and enhanced amyloid deposition *in vivo* and neuronal toxicity *in vitro*.[45] It is unknown how Aβ hexamers are structured in the interstitial space (ISS) and in the CSF.

The contribution of trimer Aβ species to the development of AD is also well documented. Stable Aβ trimers were reported in pure buffer.[46] Membrane-bound Aβ trimers correlated with toxicity towards cultured neurons,[47] and an Aβ trimer is likely the minimal oligomer size to insert into a membrane.[25] Finally, Aβ trimers were found to induce progressive loss of hippocampal synapses.[48]

2.2. Impact of Membrane on Aβ42 Intramolecular Side Chain Interactions. The intramolecular side chain contact maps were also compared. The ss-NMR fibril structure features interactions through the side chains L17, F19, F20 and V24 with the side chains A30, I32 and L34 stabilizing the packing between the β-sheets β2 and β3, and through the side chain I31 with the side chains V36, V39 and I41 stabilizing the β-sheets β4 and β5.[39] The conformations between 0 and 100 ns (Figures 4A and 4E) reveal that, averaged over the two runs, the hydrophobic

interactions stabilizing the C-terminus (residues 30-42) are still formed, but with lower lifetimes, contacts I31-V39 (probability of 75%), I31-I41 (probability of 36%) and I31-V36 (probability of 45%). The hydrophobic contacts stabilizing the interface β-sheets β2 and β3 are also partially recovered with three contacts A30-F19 (40%), I32-F19 (probability of 65%), A30-F20 (probability of 45%). In the three time-windows 500-1000, 1000-1500 and 1900-2000 ns, more non ss-NMR and a few ss-NMR contacts are formed (Figures 4B-4D and 4F-4H). The C-terminus is still stabilized by the ss-NMR contacts I31-V39 and I31-V36 in the two runs. The interface between β2 and β3 is stabilized by the ss-NMR contacts V24-A30 and F20-A30 in run 2 and by no contacts with a probability > 30% in run 1. Overall, the intrapeptide contact maps provide evidence of the significant change in the tertiary structures of Aβ oligomers embedded in a membrane model consisting of DOPC lipids.

2.3. Insertion Depths of Aβ42 Residues into the Membrane. Next, we evaluated the time evolution of the insertion depths of residues into the membrane. There is a clear difference in the insertion depth profiles between the two runs (Figure 5). In the ensemble of conformations covering the 0-100 ns time interval of the two runs, residues D1-G9 and A21-G25 are exposed to solvent and all other residues are inserted into the membrane (Figures 5A and 5C). The dynamics modifies the solvent-exposure of the residues, and the final 1900-2000 ns reveals distinct insert depths of the residues belonging to trimers 1 and 2. In run 1, residues D1-Y10(V12) and A21-G25 (A1-G29) remain exposed to solvent, the CHC is much less inserted into the membrane, residue L17 going from 0.9-1.4 nm (Figure 4A) to 1.8 nm (Figure 5B). In run 1 residues A30-A42 of trimer 2 are fully inserted into the membrane, while only residues A30-V40 of trimer 1 are fully inserted. In run 2, shown in Figure 5D, all residues D1-G29, I41 and A42 of trimer 2 have insertion depths > 2.1 nm, and the C-terminus residues 30-40 are inserted into the membrane. In contrast in trimer 1 of run 2, the CHC has insertion depths < 2.1 nm and all residues D22-A42, except L34 and M35, are solvent-exposed. Figure S1 in Supplementary Information (SI) shows that the insertion depth of each residue, averaged over 1900-2000 ns in runs 1 and 2, does not change the results if we consider each chain.

The simulations also reveal that residues 1-10 in both trimers of run 1 and in trimer 1 of run 2, and residues 1-16 in trimer 2 of run 2 are solvent-exposed due to the complex network of

interactions between the Aβ42 peptides, lipid bilayers and solvent. This result is consistent with many simulations of Aβ42 oligomers partially embedded in the membrane.[6,7,49] The N-termini appear turn/coil, and we do not find any evidence of the formation of a β-hairpin in the N-terminus, as reported for Aβ42 dimers in DOPC bilayers.[35] The high solvent accessibility of the N-terminus residues 1-16 may help understand the linking of liposomes through Aβ oligomers, as assessed by cryo-electron tomography.[50]

2.4. Membrane Deformation and Water Permeability. An important question is whether the membrane deforms and disrupts during the dynamics. Figure 6 reports on the positional probability of all lipid atoms projected on the (y,z) plane where x is the direction of the fibril axis in run 1 as a function of time. We see insertion of lipid atoms within the bilayer at y distances varying between 6 and 12 nm and z distances between 4 and 8 nm with a probability of 0.2 in the time intervals 500-1000 ns, 1000-1500 ns and 1900-2000 ns in contrast to the CHARMM-GUI starting conformation. A very similar positional probability of lipids is observed in run 2 shown in Figure 7, albeit the positional probabilities are not superposable. Differences in the membrane dynamics between the two runs are observed in the curvature and in the thinning and thickening of the membrane. The z dimension of the membrane varies between the minimal and maximal values of 2.8 and 4.7 nm in run 1 and 2.5 and 5 nm in run 2 if we consider a lipid probability of 0.3. Overall, the membrane disruption is therefore much more pronounced than that observed in simulations of Aβ42 dimer[35] and tetramer[38] in a membrane.

As a result of membrane deformation, we anticipated that waters molecules would insert into the lipid bilayer. This is supported by the positional probabilities of water molecules as a function of time intervals in particular at y distances between 8 and 12 nm and z distances between 4.5 and 7 nm in contrast to the CHARMM-GUI starting conformation. The ensemble is heterogeneous with no true dominant interpeptide and intrapeptide contacts. The MD structures of the oligomer at times 500, 1000, 1500 and 2000 ns in runs 1 and 2, shown in Figure S2, illustrate the wide variety of orientations and packings of the system from the starting structure.

The relationship between increased solvent exposure of hydrophobic residues, increased toxicity and disruption of lipid membranes was discussed for several amyloid protein systems,[51-

[53] but no long-time MD simulations and high-resolution structure experiments were conducted on Aβ42 to reveal this relationship at atomistic level. In this study, we find a structural model (trimer 2 in run 2) disrupting lipid integrity that is fully consistent with the map of the soluble Aβ40 assembly toxic surface proposed by Melacini et al., namely the solvent-exposure of the CHC region and of the loop region (residues E22-K28) and shielding of residues A30-V40 from solvent.[33] But all configurations disrupting membrane permeability do not satisfy these conditions as the CHC and C-terminus regions may be solvent-protected and solvent-exposed, respectively. Clearly exposing the C-terminus to solvent might be a template to promote fibril formation at the surface of the membrane.

It is important to discuss the initial membrane-embedded model with charged N-termini at both leaflets of the membrane. As assessed by various *in vitro* experiments, soluble oligomers in the extracellular space can adsorb and penetrate the cell membranes.[7] β-barrel models suggested by Lal et al. have all N-terminus residues located in the bulk solution at the upper membrane leaflet,[25,26] and Aβ42 fibrils can displace the upper leaflet of the membrane. In this context, using cryo-electron tomography, Viles et al. showed that Aβ42 oligomers are able to embed within the upper leaflet of the bilayer.[50] Additionally, prior to Aβ release in the extracellular space after amyloid precursor cleavage, the residues 1-27 are in the bulk solution at the upper membrane leaflet and residues 28-42 in the interior of the membrane.[7]

There is however evidence that Aβ oligomerization begins intracellularly in cells derived from human brain,[54] and there is a generation of intracellular Aβ pool.[55] In this case all N-terminus residues remain intracellular and all residues 17-42 need to cross the lower leaflet of the membrane. Finally, neutron reflection from tethered membranes showed that Aβ oligomers insert into the bilayer affecting both membrane leaflets,[56] and NMR structures of incorporated-Aβ42 β-sheet tetramer and octamer showed N-terminal residues in both the upper and lower leaflets of the membrane,[22] indicating that polar residues can cross the membrane. Overall, our initial model with charged N-terminus Aβ42 tails located in the bulk solution at the upper and lower leaflets of the membrane is supported experimentally and also corresponds to a mixture of both extracellular and intracellular aggregates, respectively.

3. CONCLUSIONS

The topic of Aβ embedding in membranes is of intense interest as the connection to Alzheimer's disease pathology is quite clear. In this study, we have determined the dynamics of a cross-β Aβ42 hexamer inserted into a neutral DOPC lipid bilayer. Using two extensive atomistic MD simulations, we showed significant changes in secondary, tertiary and quaternary structures of the cross-β model leading to two types of mainly random coil oligomers: hexamer and trimers. Both species promote an increase of the hydrophobic surface of Aβ42 peptides exposed to solvent, insertion of water molecules and lipids into the bilayer and membrane destabilization.

Membrane-embedded Aβ species with increase in membrane conductance, which do not display Thioflavin T fluorescence, consist of a wide range of conformations and oligomer sizes, some forming perfect β-barrel pores[21,25,26] or six stranded β-sheet and β-sandwich structures,[22] and others adopting spherical species without any evidence of discrete channel or pore formation.[57] Our computational work provides evidence of metastable hexamer and trimers characterized by the N-terminal residues located in the top and bottom leaflets of membrane with a minimal lifetime of several microseconds. These oligomers induce membrane permeability and water permeation that will facilitate the transport of hydrated ions from the intracellular to the extracellular space. These two assemblies, which are mainly coil/turn, are characterized by different solvent exposures of the residues. In the hexamer, we observe membrane insertion of the CHC region and residues 29-41. In the two separated trimers, we observe an increase of solvent exposure of the hydrophobic CHC and C-terminus residues.

Whether there is insertion of individual peptides which then form trimers and hexamers in the membrane or insertion of preformed trimers remains an open question, the insertion process depending in part on the physicochemical properties of the membrane.[25,58,59] Homogeneous DOPC bilayers are a simple model to represent physiological cells. It is known that POPC-POPG bilayers, and brain total lipid extracts impact Aβ adsorption, and the macroscopic ion flux across Aβ channels in membranes, respectively.[60,61] Pure DOPC bilayers also ignore the contribution of cholesterol and GM1 lipids,[7,17,34,62] and cells have extracellular matrices that result in very different behaviors compared to vesicles, liposomes and planar lipid bilayers in the absence of membrane protein receptors.[63] Going beyond DOPC bilayers and exploring

computationally other β-rich aggregates in the presence of protein receptors,[63] and free phospholipids[64-66] in the extracellular space could offer a deeper understanding of the relationship between amyloid oligomers and membrane permeability in order to develop new drugs.[53,67] In this context, new experimental methods of biomolecular processes in membrane spanning the microsecond time resolution and detecting populations of intermediates below the percent range would be very useful to validate MD-generated models.

4. MATERIAL AND METHODS

The initial structure of the hexamer Aβ42 fibril from solid state nuclear magnetic spectroscopy (ss-NMR) was taken from PDB entry 2NAO.[68] The fibril was inserted into the membrane of dimension (x =20 nm, y = 20 nm, z = 4.2 nm), and its orientation was selected to maximize the total number of hydrophobic CHC (L17-A21) and C-terminal (A30-A42) residues inserted into the membrane and the total number of polar/charged residues exposed to solvent. The bilayer, consisting of 1128 DOPC (neutral) lipids, was immersed in a box of 20 nm, 20 nm and 12.1 nm with about 99000 water molecules. Simulations were performed at pH 7. Aβ42 peptides have $NH3^+$ and $CO2^-$ termini, deprotonated Glu and Asp, protonated Arg and Lys, and neutral His with a protonated N_ε atom. The system was neutralized by sodium ions leading to a total number of about 456000 atoms. CHARMM-GUI was used to set up the system.[69] Figure 1 shows the initial structure of the hexamer generated by CHARMM-GUI with C2 symmetric molecules. Residues D1-E11 and E22-V24 are exposed to solvent, residues Q15-F20 and K28-A42 are embedded in the membrane, and residues V12-H14 and G25-N27 are in the subspace formed by head and glycerol lipid groups. It has to be noted the N-terminal residues of three chains are located in aqueous solution at the upper leaflet of the membrane (these three chains will be referred to as trimer 1) and the N-terminal residues of other three chains (referred to as trimer 2) are located in aqueous solution at the lower leaflet of the membrane.

The CHARMM36 force field was used for the Aβ42 peptides and the lipids,[70] and water molecules were modelled by the CHARMM-modified TIP3P model.[71] CHARMM36m, refined for intrinsically disordered proteins in the bulk solution, was not used because its relevance on transmembrane proteins remains to be determined.[71] Two MD simulations of 2 μs were

performed at 303 K (run 1) and 310 K (run 2) in the NPT ensemble as a single simulation, regardless of its length, is not sufficient to show that the results are reliable or may be an artefact. The choice of 310 K is also motivated by the fact that 2 μs at 303 K might be too short to see major oligomeric changes and two simulations at the same temperature starting from the same configurations with different starting velocities might not be adequate. Also, the use of two slightly different temperatures allows a better sampling of the configurational space. In this study, we used GROMACS (version 2019.4),[72] and a time step of 2 fs with the lengths of bonds with hydrogen atoms constrained using the LINCS algorithm.[73] Minimization and equilibration of 1 ns were performed with restraints on the backbone atoms of Aβ42 peptides. Temperature and pressure were controlled using the Noose-Hoover algorithm with a coupling constant of 1 ps,[74] and the semi-isotropic Parrinello-Rahman algorithm with a coupling constant of 5 ps,[75] respectively. Electrostatic interactions were calculated using the particle mesh Ewald method with a cutoff of 1.2 nm, and Van der Waals interactions used forces switched to zero from 1.0 to 1.2 nm, as implemented in CHARMM-GUI.[69]

Prior to analysis, we emphasize that the protonation states we assigned assume canonical (solution) pKa values. While most of the polar/charged residues are initially exposed to solvent and notably the N-terminal residues and residues E22 and D23, K28 is embedded in the membrane. It is known that Lysine can shift its pKa down to 6 in hydrophobic environments, e.g., when fully inserted in a membrane.[76] In our starting structure, as K28 partially feels the presence of the head and glycerol lipid groups, its pKa value is unknown. Assuming therefore that K28 is protonated is an approximation which might not be totally appropriate. In principle, we can solve this issue by using pH-replica exchange MD simulations, but this approach is not computationally feasible for a hexamer of 252 amino acids partially embedded in an atomistic lipid bilayer.

To characterize the conformational ensemble, secondary structures were determined using the DSSP method.[77] Conformations were characterized by their intra and intermolecular (between trimer 1 and trimer 2) contact maps. A contact between two side chains was considered formed if there is at least one distance < 0.45 nm between all heavy atoms. We calculated the average depth of residues 1-42 into the lipid bilayer. One residue was considered inserted if the depth is < 2.1 nm. The insertion depth was calculated as the z component of the distance

between the center of mass of each residue (including all backbone and side chain atoms) and the center of mass of all lipid atoms of the membrane.[78] Finally, we also calculated the positional probabilities of the lipids and water molecules with respect to the membrane surface.

ASSOCIATED CONTENT

Supporting Information.

The Supporting Information is available free of charge at https://pubs.acs.org/doi/
Insertion depths of residues 1-42 belonging to each chain of the system in the time-interval 1900-2000 ns of run 1 and run 2, and snapshots of the system as a function of time in runs 1 and 2 are reported.

AUTHOR INFORMATION

Corresponding Author

*E-mail: philippe.derreumaux@ibpc.fr

ORCID

Phuong H. Nguyen: 0000-0003-1284-967X, phuong.nguyen@ibpc.fr

Philippe Derreumaux: 0000-0001-9110-5585

Author Contributions

P.D conceived the research. P.H.N performed the simulations. P.H. N. and P.D analyzed the results. P.H. N. and P.D. wrote the paper.

Notes

The authors declare no competing financial interest.

ACKNOWLEDGMENTS. This work was supported by grants from the French IDRIS and CINES computer centers, and the “Initiative d’Excellence” program from the French State, Grant “DYNAMO”, ANR-11-LABX-0011.

References

1. Dobson, C.M. Protein Misfolding, Evolution and Disease. *Trends Biochem Sci.* **1999**, *24*, 329-332.
2. Nasica-Labouze, J.; Nguyen, P.H.; Sterpone, F.; Berthoumieu, O.; Buchete, N.V.; Coté, S.; De Simone, A.; Doig, A.J.; Faller, P.; Garcia, A. et al. Amyloid β Protein and Alzheimer's Disease: When Computer Simulations Complement Experimental Studies. *Chem Rev.* **2015**, *115*, 3518-3563.
3. Arai, M.; Sugase, K.; Dyson, H.J.; Wright, P.E. Conformational Propensities of Intrinsically Disordered Proteins Influence the Mechanism of Binding and Folding. *Proc Natl Acad Sci U S A.* **2015**, *112*, 9614-9619.
4. Nguyen, P.H.; Derreumaux, P. Structures of the Intrinsically Disordered Aβ, tau and α-synuclein Proteins in Aqueous Solution from Computer Simulations. *Biophys. Chem.* **2020**, *264,* 106421.
5. Quist, A.; Doudevski, I.; Lin, H.; Azimova, R.; Ng, D.; Frangione, B.; Kagan, B.; Ghiso, J.; Lal, R. Amyloid Ion Channels: A Common Structural Link for Protein-misfolding Disease. *Proc. Natl. Acad. Sci. U. S. A* **2005**, *102*, 10427-10432.
6. Liu, Y.; Ren, B.; Zhang, Y.; Sun, Y.; Chang, Y.; Liang, G.; Xu, L.; Zheng; J. Molecular Simulation Aspects of Amyloid Peptides at Membrane Interface. *Biochim Biophys Acta Biomembr.* **2018**, *1860,* 1906-1916.
7. Nguyen, P.H.; Ramamoorthy, A.; Sahoo, B.R.; Zheng, J.; Faller, P.; Straub, J.E, Dominguez, L.; Shea, J.E.; Dokholyan, N.V.; De Simone, A. et al. Amyloid Oligomers: A Joint Experimental/Computational Perspective on Alzheimer's Disease, Parkinson's Disease, Type II Diabetes, and Amyotrophic Lateral Sclerosis. *Chem Rev.* **2021**, *121*, 2545-2647.
8. Gonzalez-Garcia, M.; Fusco, G.; De Simone, A. Membrane Interactions and Toxicity by Misfolded Protein Oligomers. *Front Cell Dev Biol.* **2021**, *9*, 642623.
9. Berthelot, K.; Cullin, C.; Lecomte, S. What Does Make an Amyloid Toxic: Morphology, Structure or Interaction with Membrane? *Biochimie.* **2013**, *95*, 12-9.
10. Ait-Bouziad, N.; Lv, G.; Mahul-Mellier, A.L.; Xiao, S.; Zorludemir, G.; Eliezer, D.; Walz, T.; Lashuel, H.A. Discovery and Characterization of Stable and Toxic Tau/phospholipid Oligomeric Complexes. *Nat. Commun.* **2017**, *8*, 1678.
11. Lasagna-Reeves, C.A.; Sengupta, U.; Castillo-Carranza, D.; Gerson, J.E.; Guerrero-Munoz, M.; Troncoso, J.C.; Jackson, G.R.; Kayed, R. The Formation of Tau Pore-like Structures is Prevalent and Cell Specific: Possible Implications for the Disease Phenotypes. *Acta Neuropathol Commun.* **2014**, *2*, 56.
12. Di Scala, C.; Yahi, N.; Boutemeur, S.; Flores, A.; Rodriguez, L.; Chahinian, H.; Fantini, J. Common Molecular Mechanism of Amyloid Pore Formation by Alzheimer's β-amyloid Peptide and α-synuclein. *Sci. Rep*. **2016***, 6*, 28781.
13. Arispe, N.; Pollard, H.B.; Rojas, E. Giant Multilevel Cation channels Formed by Alzheimer Disease Amyloid Beta-protein [A beta P-(1-40)] in Bilayer Membranes. *Proc Natl Acad Sci U S A.* **1993**, *90*, 10573-10577.
14. Durell, S. R., Guy, H. R., Arispe, N., Rojas, E., Pollard, H. B. Theoretical Models of the Ion Channel Structure of Amyloid Beta-protein. *Biophys. J.* **1994**, *67*, 2137–2145.

15. Shafrir, Y., Durell, S., Arispe, N., Guy, H. R. Models of Membrane-bound Alzheimer's Abeta Peptide Assemblies. *Proteins* **2010,** *78*, 3473–3487.
16. Serra-Batiste, M.; Ninot-Pedrosa, M.; Bayoumi, M.; Gairí, M.; Maglia, G.; Carulla, N. Aβ42 Assembles into Specific β-Barrel Pore-forming Oligomers in Membrane-mimicking Environments. *Proc Natl Acad Sci U S A*. **2016**, *113*, 10866-10871.
17. Nguyen, P.H.; Campanera, J.M.; Ngo, S.T.; Loquet, A.; Derreumaux, P. Tetrameric Aβ40 and Aβ42 β-Barrel Structures by Extensive Atomistic Simulations. I. In a Bilayer Mimicking a Neuronal Membrane. *J. Phys. Chem. B.* **2019**, *123,* 3643-3648.
18. Ngo, S. T., Nguyen, P. H., Derreumaux, P. Impact of the Rat R5G, Y10F, and H13R Mutations on Tetrameric Aβ42 β-Barrel in a Lipid Bilayer Membrane Model. *J. Phys. Chem. B.* **2021**, *125*, 3105–3113.
19. Ngo, S.T.; Nguyen, P.H.; Derreumaux, P. Impact of A2T and D23N Mutations on Tetrameric Aβ42 Barrel within a Dipalmitoylphosphatidylcholine Lipid Bilayer Membrane by Replica Exchange Molecular Dynamics. *J. Phys. Chem. B.* **2020**, *124*, 1175-1182.
20. Kreutzer, A.G.; Nowick, J.S. Elucidating the Structures of Amyloid Oligomers with Macrocyclic β-Hairpin Peptides: Insights into Alzheimer's Disease and Other Amyloid Diseases. *Acc. Chem. Res.* **2018**, *51*, 706-718.
21. Österlund, N.; Moons, R.; Ilag, L.L.; Sobott, F.; Gräslund, A. Native Ion Mobility-Mass Spectrometry Reveals the Formation of β-Barrel Shaped Amyloid-β Hexamers in a Membrane-Mimicking Environment*. J. Am. Chem. Soc.* **2019,** *141*, 10440-10450.
22. Ciudad, S.; Puig, E.; Botzanowski, T.; Meigooni, M.; Arango, A.S.; Do, J.; Mayzel, M.; Bayoumi, M.; Chaignepain, S.; Maglia, G. et al. Aβ(1-42) Tetramer and Octamer Structures Reveal Edge Conductivity Pores as a Mechanism for Membrane Damage. *Nat. Commun*. **2020**, *11*, 3014.
23. Durell, S.R.; Kayed, R.; Guy, H.R. The Amyloid Concentric β-Barrel Hypothesis: Models of Amyloid beta 42 Oligomers and Annular Protofibrils. *Proteins.* **2022**, *90*, 1190-1209.
24. Ngo, S. T.; Derreumaux, P.; Vu, V. V. Probable Transmembrane Amyloid α-Helix Bundles Capable of Conducting Ca^{2+} Ions. *J. Phys. Chem. B* **2019,** *123*, 2645–2653.
25. Jang, H.; Connelly, L.; Arce, F. T.; Ramachandran, S.; Kagan, B. L.; Lal, R.; Nussinov, R. Mechanisms for the Insertion of Toxic, Fibril-like β-Amyloid Oligomers into the Membrane. *J Chem Theory Comput.* **2013**, *9*, 822–833.
26. Jang, H.; Arce, F.T.; Ramachandran, S.; Kagan, B.L.; Lal, R.; Nussinov, R. Disordered Amyloidogenic Peptides May Insert into the Membrane and Assemble into Common Cyclic Structural Motifs. *Chem Soc Rev*. **2014**, *43*, 6750-6764.
27. Jang, H.; Teran Arce, F.; Ramachandran, S.; Capone, R.; Lal, R.; Nussinov, R. Structural Convergence among Diverse, Toxic Beta-sheet Ion Channels. *J Phys Chem B.* **2010**, *114*, 9445-9451.
28. Strodel, B.; Lee, J.W.; Whittleston, C.S.; Wales, D.J. Transmembrane Structures for Alzheimer's Aβ(1-42) Oligomers. *J Am Chem Soc*. **2010**, *132*, 13300-13312.

29. Ngo ST, Nguyen PH, Derreumaux P. Stability of Aβ11-40 Trimers with Parallel and Antiparallel β-Sheet Organizations in a Membrane-Mimicking Environment by Replica Exchange Molecular Dynamics Simulation. *J Phys Chem B.* **2020**, *124*, 617-626.
30. Milanesi, L.; Sheynis, T.; Xue, W.F.; Orlova, E.V.; Hellewell, A.L.; Jelinek, R.; Hewitt, E.W.; Radford, S.E.; Saibil, H.R. Direct Three-dimensional Visualization of Membrane Disruption by Amyloid Fibrils. *Proc Natl Acad Sci U S A.* **2012**, *109*, 20455-20460.
31. Bode, D.C.; Freeley, M.; Nield, J.; Palma, M.; Viles, J.H. Amyloid-β Oligomers have a Profound Detergent-like Effect on Lipid Membrane Bilayers by Atomic Force and Electron Microscopy. *J Biol Chem.* **2019**, *294*, 7566-7572.
32. Qiang, W.; Doherty, K.E.; Klees, L.M.; Tobin-Miyaji, Y. Time-Dependent Lipid Dynamics, Organization and Peptide-Lipid Interaction in Phospholipid Bilayers with Incorporated β-Amyloid Oligomers. *J Phys Chem Lett.* **2020**, *11*, 8329-8336.
33. Ahmed, R.; Akcan, M.; Khondker, A.; Rheinstädter, M.C.; Bozelli, J.C. Jr.; Epand, R.M.; Huynh, V.; Wylie, R.G.; Boulton, S.; Huang, J. et al. Atomic Resolution Map of the Soluble Amyloid beta Assembly Toxic Surfaces. *Chem Sci.* **2019,** *10*, 6072-6082.
34. Fatafta, H.; Khaled, M.; Owen, M.C.; Sayyed-Ahmad, A.; Strodel, B. Amyloid-β Peptide Dimers Undergo a Random Coil to β-sheet Transition in the Aqueous Phase but not at the Neuronal Membrane. *Proc Natl Acad Sci U S A.* **2021**, *118*, e2106210118.
35. Press-Sandler, O.; Miller, Y. Molecular Insights into the Primary Nucleation of Polymorphic Amyloid β Dimers in DOPC Lipid Bilayer Membrane. *Protein Sci.* **2022**, *31*, e4283.
36. Nguyen, H.L.; Linh, H.Q.; Krupa, P.; La Penna, G.; Li, M.S. Amyloid β Dodecamer Disrupts the Neuronal Membrane More Strongly than the Mature Fibril: Understanding the Role of Oligomers in Neurotoxicity. *J Phys Chem B.* **2022**, *126*, 3659-3672.
37. Poojari C, Xiao D, Batista VS, Strodel B. Membrane Permeation Induced by Aggregates of Human Islet Amyloid Polypeptides. *Biophys J.* **2013**, *105*, 2323-2332.
38. Poojari C, Kukol A, Strodel B. How the Amyloid-β Peptide and Membranes Affect Each Other: An Extensive Simulation Study. *Biochim Biophys Acta.* **2013**, *1828*, 327-339.
39. Wälti, M.A.; Ravotti, F.; Arai, H.; Glabe, C.G.; Wall, J.S.; Böckmann, A.; Güntert, P.; Meier, B.H.; Riek, R. Atomic-resolution Structure of a Disease-relevant Aβ(1-42) Amyloid Fibril. *Proc Natl Acad Sci U S A.* **2016**, *113*, E4976-E4984.
40. Ghosh, U.; Thurber, K.R.; Yau, W.M.; Tycko, R. Molecular Structure of a Prevalent Amyloid-β Fibril Polymorph from Alzheimer's Disease Brain Tissue. *Proc Natl Acad Sci U S A.* **2021**, *118*, e2023089118.
41. Gallardo, R.; Iadanza, M.G.; Xu, Y.; Heath, G.R.; Foster, R.; Radford, S.E.; Ranson, N.A. Fibril Structures of Diabetes-related Amylin Variants Reveal a Basis for Surface-templated Assembly. *Nat Struct Mol Biol.* **2020**, *27*, 1048-1056.
42. Röder,C.; Kupreichyk, T.; Gremer, L.; Schäfer, L.U.; Pothula, K.R.; Ravelli, R.B.G.; Willbold, D.; Hoyer, W.; Schröder, G.F. Cryo-EM Structure of Islet Amyloid Polypeptide Fibrils Reveals Similarities with Amyloid-β fibrils. *Nat Struct Mol Biol.* **2020**, *27,* 660-667.

43. Economou, N.J.; Giammona, M.J.; Do, T.D; Zheng, X.; Teplow, D.B.; Buratto, S.K.; Bowers, M.T. Amyloid β-Protein Assembly and Alzheimer Disease: Dodecamers of Aβ42, but Not of Aβ40, Seed Fibril Formation*. J Am Chem Soc.* **2016,** *138*, 1772-1775.
44. Wolff, M.; Zhang-Haagen, B.; Decker, C.; Barz, B.; Schneider, M.; Biehl, R.; Radulescu, A.; Strodel, B.; Willbold, D.; Nagel-Steger, L. Aβ42 Pentamers/Hexamers are the Smallest Detectable Oligomers in Solution. *Sci Rep*. **2017,** *7*, 2493.
45. Vrancx, C.; Vadukul, D.M.; Suelves, N.; Contino, S.; D'Auria, L.; Perrin, F.; van Pesch, V.; Hanseeuw, B.; Quinton, L.; Kienlen-Campard, P. Mechanism of Cellular Formation and In Vivo Seeding Effects of Hexameric β-Amyloid Assemblies. *Mol Neurobiol.* **2021,** *58*, 6647-6669.
46. Chen, Y.R.; Glabe, C.G. Distinct Early Folding and Aggregation Properties of Alzheimer Amyloid-beta Peptides Abeta40 and Abeta42: Stable Trimer or Tetramer Formation by Abeta42. *J Biol Chem.* **2006**, *281*, 24414-24422.
47. Jana, M.K.; Cappai, R.; Pham, C.L.; Ciccotosto, G.D. Membrane-bound Tetramer and Trimer Aβ Oligomeric Species Correlate with Toxicity towards Cultured Neurons. *J Neurochem.* **2016,** *136*, 594-608.
48. Shankar, G.M.; Bloodgood, B.L.; Townsend, M.; Walsh, D.M.; Selkoe, D.J.; Sabatini, B.L. Natural Oligomers of the Alzheimer Amyloid-beta Protein Induce Reversible Synapse Loss by Modulating an NMDA-type Glutamate Receptor-dependent Signaling Pathway. *J Neurosci.* **2007**, *27*, 2866-2875.
49. Feng, W.; Lei, H.; Si, J.; Zhang, T. Study of Structural Stability and Damaging Effect on Membrane for four Aβ42 Dimers. *PLoS One*. **2017,** *12*, e0179147.
50. Tian, Y.; Liang, R.; Kumar, A.; Szwedziak, P.; Viles, J.H. 3D-visualization of Amyloid-β Oligomer Interactions with Lipid Membranes by Cryo-electron Tomography. *Chem Sci.* **2021,** *12*, 6896-6907.
51. Capitini, C.; Patel, J.R. ; Natalello, A.; D'Andrea, C. ; Relini, A. ; Jarvis, J.A. ; Birolo, L. ; Peduzzo, A. ; Vendruscolo, M. ; Matteini, P. et al. Structural Differences between Toxic and Nontoxic HypF-N Oligomers. *Chem Commun (Camb).* **2018**, *54,* 8637-8640.
52. Ladiwala, A.R.; Litt, J.; Kane, R.S.; Aucoin, D.S.; Smith, S.O.; Ranjan, S.; Davis, J.; Van Nostrand, W.E.; Tessier, P.M. Conformational Differences between Two amyloid β Oligomers of Similar Size and Dissimilar Toxicity. *J Biol Chem.* **2012**, *287*, 24765-24773.
53. Errico, S. ; Ramshini, H. ; Capitini, C. ; Canale, C. ; Spaziano, M. ; Barbut, D. ; Calamai, M. ; Zasloff, M. ; Oropesa-Nuñez, R. ; Vendruscolo, M. et al. Quantitative Measurement of the Affinity of Toxic and Nontoxic Misfolded Protein Oligomers for Lipid Bilayers and of its Modulation by Lipid Composition and Trodusquemine. *ACS Chem Neurosci.* **2021**, *12*, 3189-3202.
54. Walsh, D.M.; Tseng, B.P.; Rydel, R.E.; Podlisny, M.B.; Selkoe, D.J. The Oligomerization of Amyloid beta-protein Begins Intracellularly in Cells Derived from Human Brain. *Biochemistry.* **2000**, *39*, 10831-10839.
55. Sannerud, R.; Esselens, C. ; Ejsmont, P. ; Mattera, R. ; Rochin, L. ; Tharkeshwar, A.K. ; De Baets, G. ; De Wever, V. ; Habets, R. ; Baert, V. et al. Restricted Location of PSEN2/γ-

Secretase Determines Substrate Specificity and Generates an Intracellular Aβ Pool. *Cell.* **2016**, *166*, 193-208.
56. Valincius, G.; Heinrich, F.; Budvytyte, R.; Vanderah, D.J.; McGillivray, D.J.; Sokolov, Y.; Hall, J.E.; Lösche, M. Soluble Amyloid Beta-oligomers Affect Dielectric Membrane Properties by Bilayer Insertion and Domain Formation: implications for Cell Toxicity. *Biophys J.* **2008**, *95*, 4845-4861.
57. Kayed, R.; Sokolov, Y.; Edmonds, B.; McIntire, T.M.; Milton, S.C.; Hall, J.E.; Glabe, C.G. Permeabilization of Lipid Bilayers is a Common Conformation-dependent Activity of Soluble Amyloid Oligomers in Protein Misfolding Diseases. *J Biol Chem.* **2004**, *279*, 46363-46366.
58. Arce, F.T.; Jang, H.; Ramachandran, S.; Landon, P.B.; Nussinov, R.; Lal, R. Polymorphism of Amyloid β Peptide in Different Environments: Implications for Membrane Insertion and Pore Formation. *Soft Matter.* **2011**, *7*, 5267-5273.
59. Kleinschmidt, J.H. Folding of β-barrel Membrane Proteins in Lipid Bilayers - Unassisted and Assisted Folding and Insertion. *Biochim Biophys Acta.* **2015**, *1848*, 1927-1943.
60. Yu, X.; Wang, Q.; Pan, Q.; Zhou, F.; Zheng, J. Molecular Interactions of Alzheimer Amyloid-β Oligomers with Neutral and Negatively Charged Lipid Bilayers. *Phys Chem Chem Phys.* **2013**, *15*, 8878-8889.
61. Lee, J.; Kim, Y.H.; T Arce, F.; Gillman, A.L.; Jang, H.; Kagan, B.L.; Nussinov, R.; Yang, J.; Lal, R. Amyloid β Ion Channels in a Membrane Comprising Brain Total Lipid Extracts. *ACS Chem Neurosci.* **2017**, *8*, 1348-1357.
62. Nguyen PH, Sterpone F, Derreumaux P. Self-Assembly of Amyloid-Beta (Aβ) Peptides from Solution to Near *In Vivo* Conditions. *J Phys Chem B.* **2022**, *126*, 10317-10326.
63. Sakono, M.; Zako, T. Amyloid Oligomers: Formation and Toxicity of Abeta Oligomers. *FEBS J.* **2010**, *277,* 1348-1358.
64. Ngo, S.T.; Nguyen, P.H.; Derreumaux, P. Cholesterol Molecules Alter the Energy Landscape of Small Aβ1-42 Oligomers. *J Phys Chem B.* **2021**, *125*, 2299-2307.
65. Nguyen, T.H.; Nguyen, P.H.; Ngo, S.T.; Derreumaux, P. Effect of Cholesterol Molecules on Aβ1-42 Wild-Type and Mutants Trimers. *Molecules.* **2022**, *27*, 1395.
66. Chakravorty, A.; McCalpin, S.D.; Sahoo, B.R.; Ramamoorthy, A.; Brooks, C.L. 3rd. Free Gangliosides Can Alter Amyloid-β Aggregation. *J Phys Chem Lett.* **2022**, *13*, 9303-9308.
67. Doig, A.J.; Del Castillo-Frias, M.P.; Berthoumieu, O.; Tarus, B.; Nasica-Labouze, J.; Sterpone, F.; Nguyen, P.H.; Hooper, N.M.; Faller, P.; Derreumaux, P. Why Is Research on Amyloid-β Failing to Give New Drugs for Alzheimer's Disease? *ACS Chem. Neurosci.* **2017**, *8*, 1435-1437.
68. Berman, H.M.; Westbrook, J.; Feng, Z.; Gilliland, G.; Bhat, T.N.; Weissig, H.; Shindyalov, I.N.; Bourne, P.E. The Protein Data Bank. *Nucleic Acids Res.* **2000**, *28,* 235-242.
69. Lee, J.; Cheng, X.; Swails, J.M.; Yeom, M.S.; Eastman, P.K.; Lemkul, J.A.; Wei, S.; Buckner, J.; Jeong, J.C.; Qi; Y. et al. CHARMM-GUI Input Generator for NAMD, GROMACS, AMBER, OpenMM, and CHARMM/OpenMM Simulations Using the CHARMM36 Additive Force Field. *J Chem Theory Comput.* ***2016,*** *12*, 405-413.

70. Pastor, R.W.; Mackerell, A.D. Jr. Development of the CHARMM Force Field for Lipids. *J Phys Chem Lett.* **2011**, *2*, 1526-1532.
71. Huang, J.; Rauscher, S.; Nawrocki, G.; Ran, T.; Feig, M.; de Groot, B.L.; Grubmüller, H.; MacKerell, AD Jr. CHARMM36m: An Improved Force Field for Folded and Intrinsically Disordered Proteins. *Nat Methods.* **2017,** *14*, 71-73.
72. van der Spoel, D.; Lindahl, E.; Hess, B.; Groenhof, G.; Mark, A. E.; Berendsen, H. J. GROMACS: Fast, Flexible, and Free. *J. Comput. Chem.* **2005**, *26*, 1701−1718.
73. Hess, B.; Bekker, H.; Berendsen, H.J.C.; Fraaije, J.G.E.M. LINCS: a Linear Constraint Solver for Molecular Simulations. *J. Comp. Chem.* **1997**, *18*, 1463-1472.
74. Evans, D.J., Holian, B.L. The Nose-Hoover Thermostat. *J. Chem. Phys.* **1985**, *83*, 4069.
75. Parrinello, M.; Rahman, A. Polymorphic Transitions in Single Crystals: A new Molecular Dynamics Method. *J. Appl. Phys.* **1981**, *52*, 7182-7190.
76. Panahi, A.; Brooks, C.L. 3rd. Membrane Environment Modulates the pKa Values of Transmembrane Helices. *J Phys Chem B.* **2015**, *119*, 4601-4607.
77. Kabsch, W.; Sander, C. Dictionary of Protein Secondary Structure: Pattern Recognition of Hydrogen-bonded and Geometrical Features. *Biopolymers* **1983**, *22*, 2577-2637.
78. Nguyen PH, Derreumaux P. Molecular Dynamics Simulations of the Tau Amyloid Fibril Core Dimer at the Surface of a Lipid Bilayer Model: I. In Alzheimer's Disease. *J Phys Chem B.* **2022**, *126*, 4849-4856.

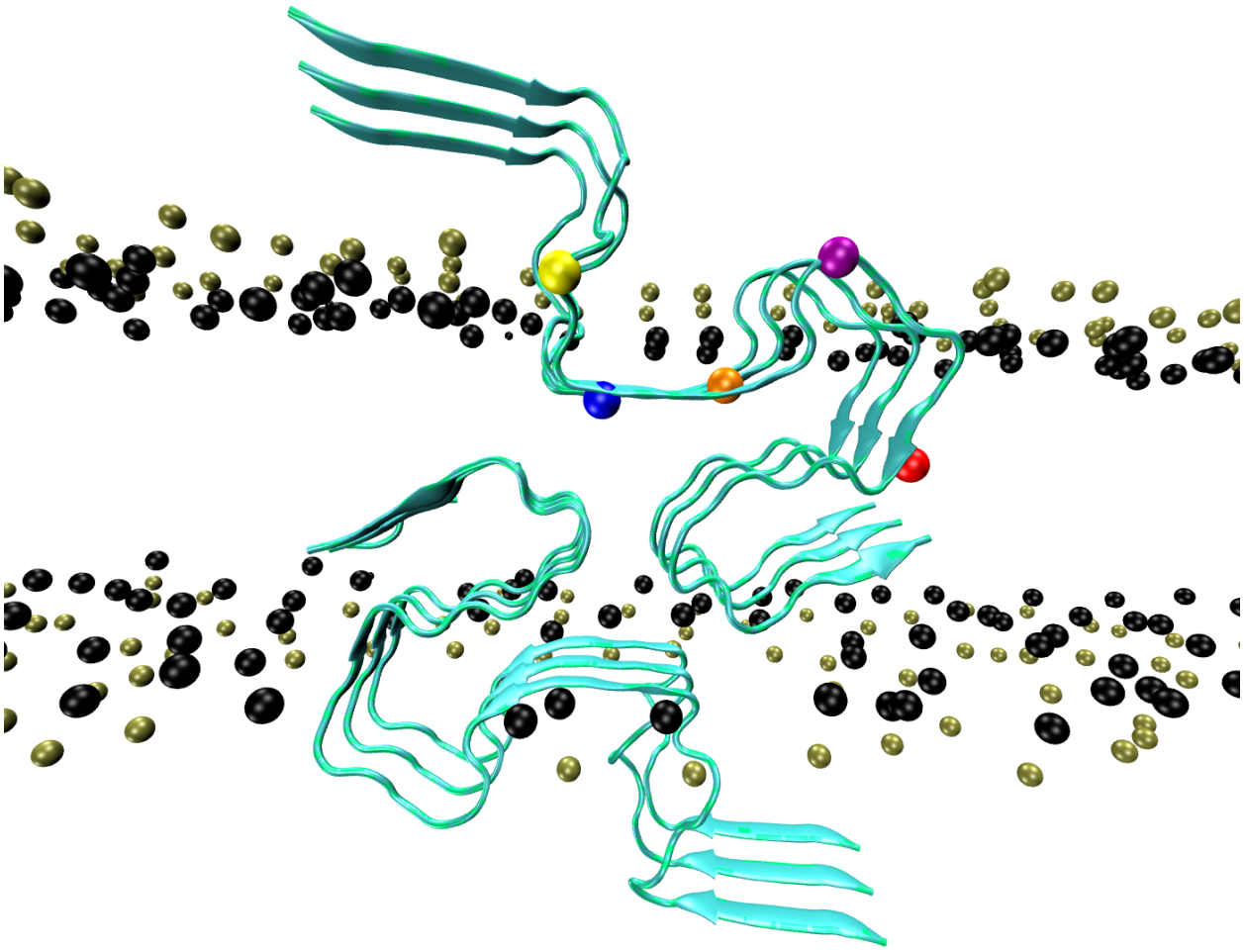

Figure 1. Initial CHARMM-GUI conformation of the system. View in the x direction parallel to the fibril axis. We show the ribbon structure of the hexamer, the phosphate atoms (tan) and the O21 and O22 atoms of the glycerol (black). Also shown are the Cα atom of V12 (yellow), Q15 (blue), V18 (orange), E22 (purple) and K28 (red).

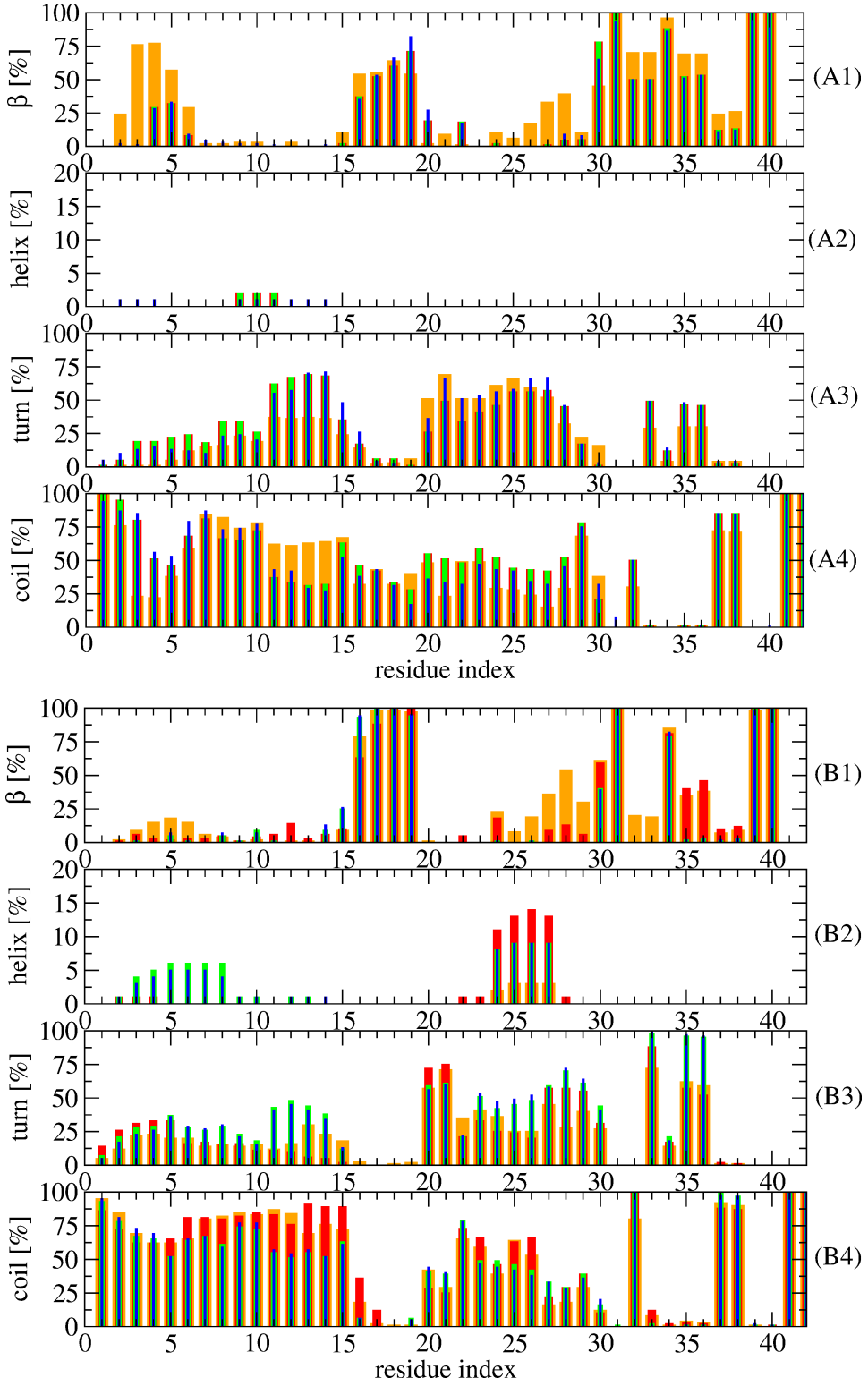

Figure 2. Time-averaged secondary structure contents along the sequence using four time-windows of run 1 at 303 K (A1, A2, A3, A4) and run 2 at 310 K (B1, B2, B3, B4) using 0-500 ns (orange), 500-1000 ns (red), 1000-1500 ns (green) and 1500-2000 ns (blue).

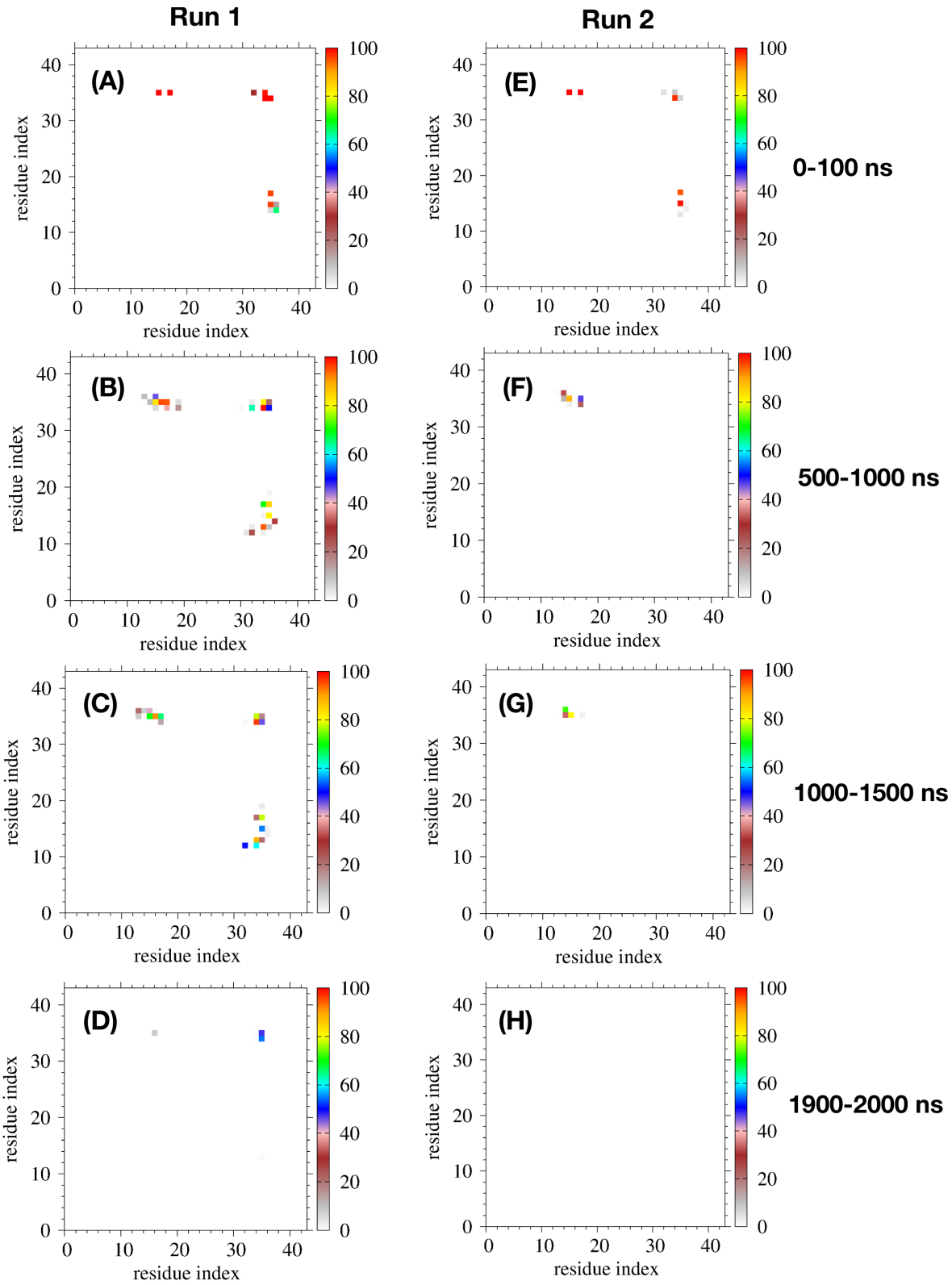

Figure 3. Intermolecular side chain contact map probabilities as a function of time intervals for the two runs, run 1 at 303 K and run 2 at 310 K.

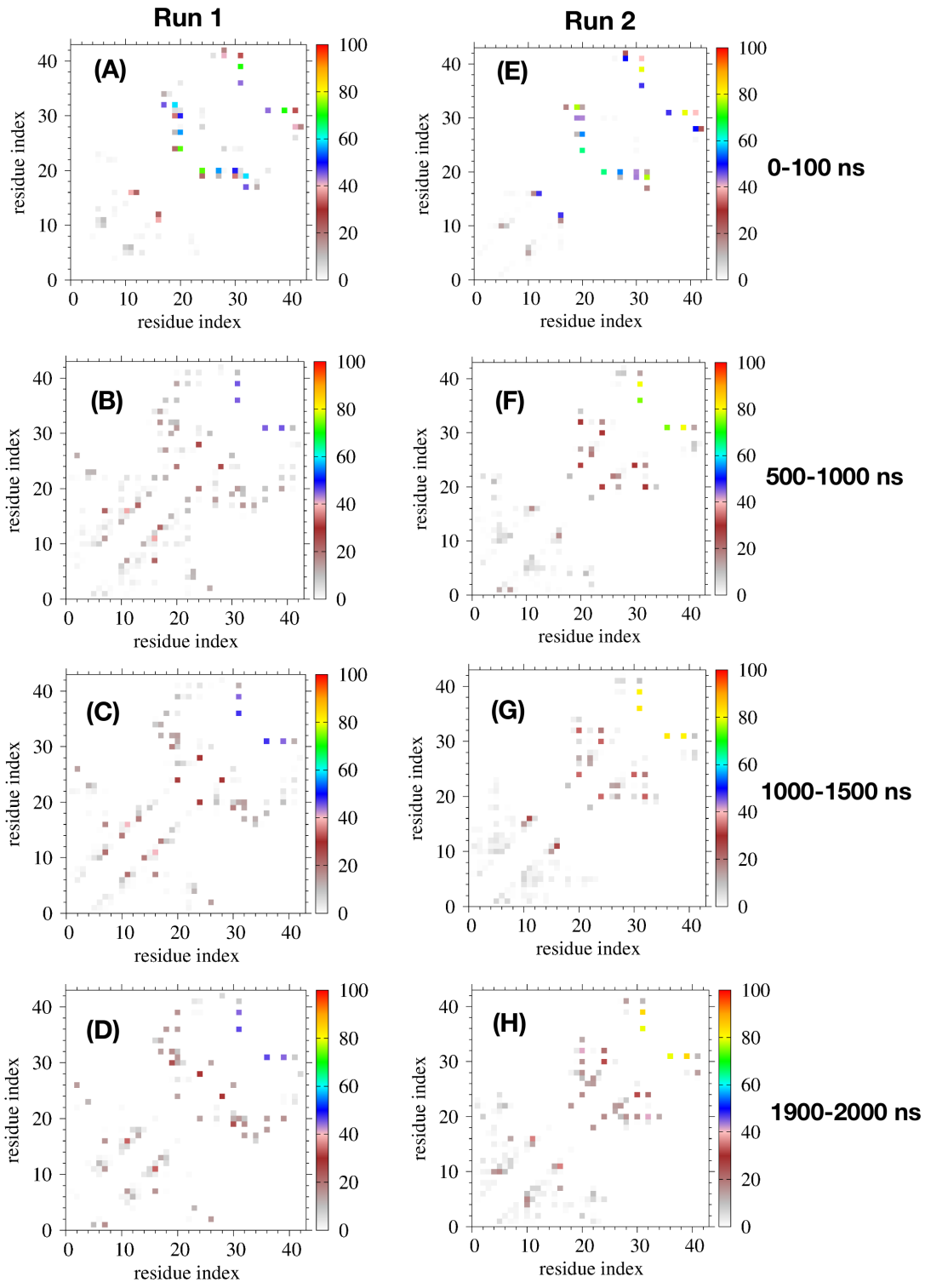

Figure 4. Intramolecular side chain contact map probabilities as a function of time intervals for the two runs (run 1 at 303 K and run 2 at 310 K) separated at least by four residues.

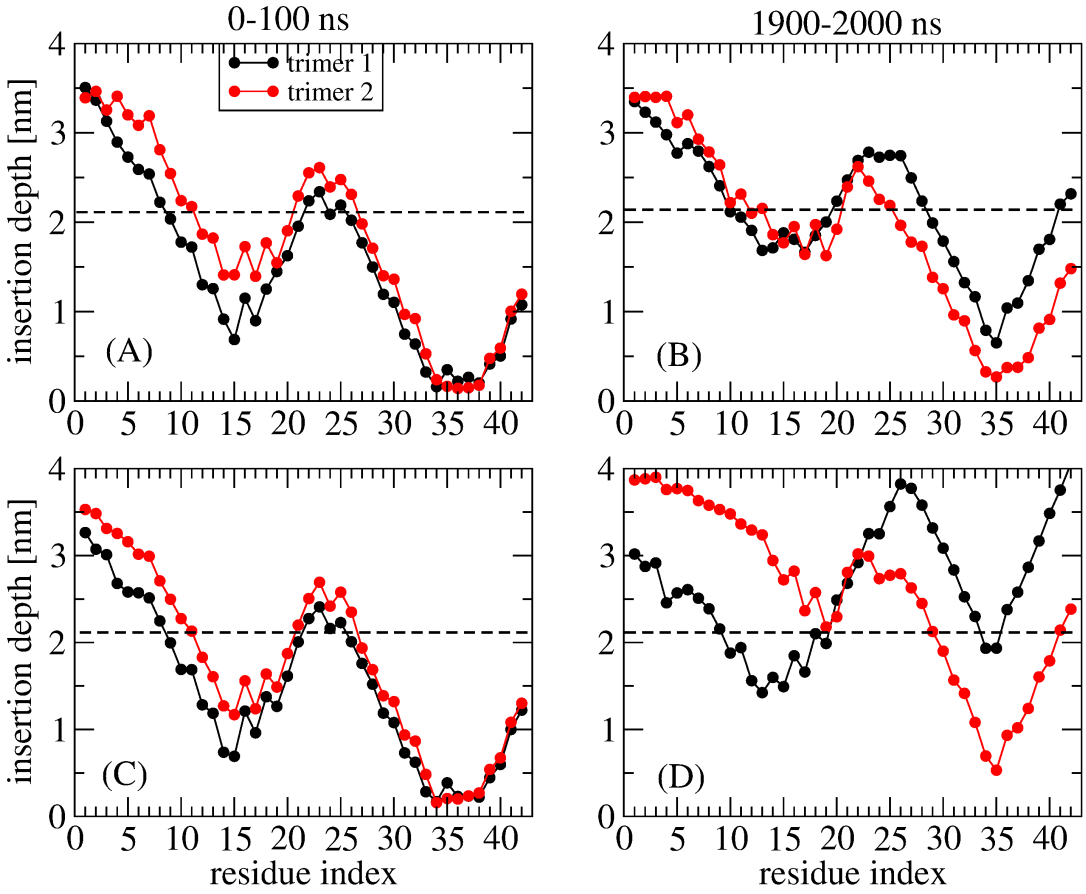

Figure 5. Insertion depths of the residues belonging to trimer 1 and trimer 2 in two time-intervals, 0-100 ns and 1900-2000 ns. (A) and (B) refer to run 1 at 303 K, and (C) and (D) to run 2 at 310 K.

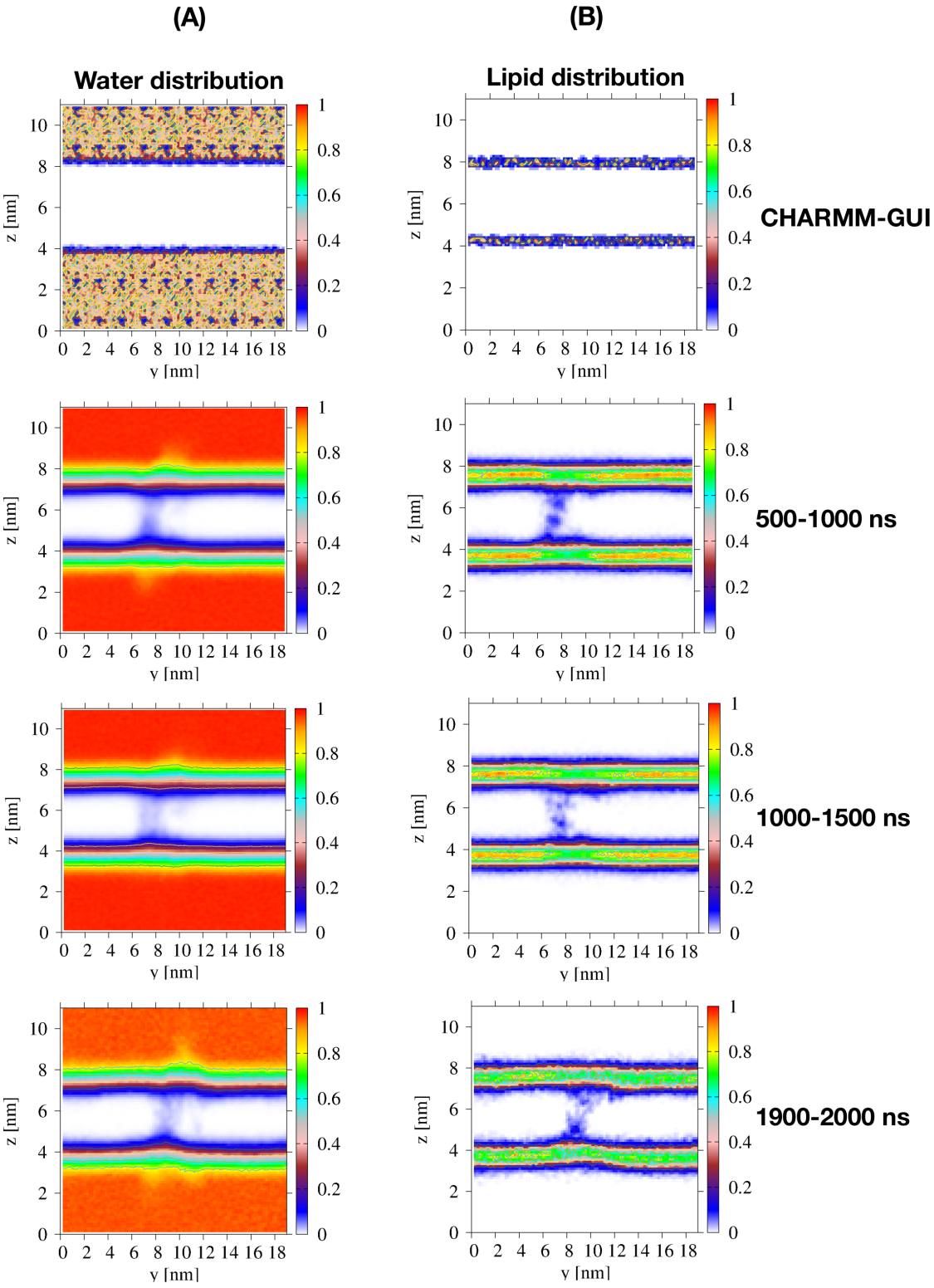

Figure 6. Run 1 (303 K) simulation results of water (A) and lipid (B) positional probabilities projected on the (y,z) plane where x is fibril axis. We show the CHARMM-GUI values, free of equilibration, and the averaged values using three time-intervals.

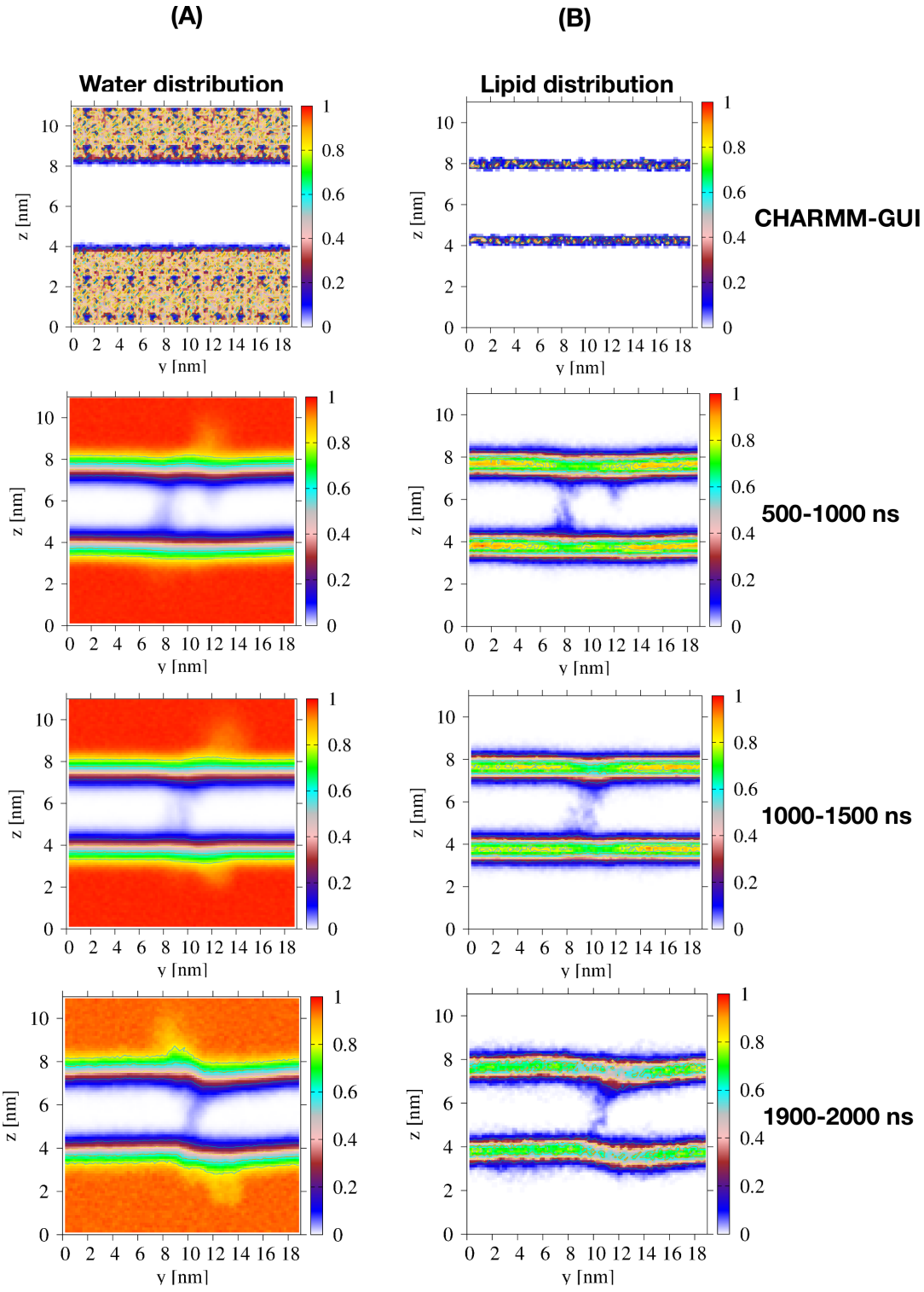

Figure 7. Run 2 (310 K) simulation results of water and lipid positional probabilities projected on the (y,z) plane where x is fibril axis. We show the CHARMM-GUI values, free of equilibration, and the averaged values using three time-intervals.

For Table of Contents Use Only

A S-shaped Aβ42 Cross-β Hexamer Embedded into a Lipid Bilayer Reveals Membrane Disruption and Permeability

Phuong H Nguyen,[1] and Philippe Derreumaux [1,2*]